# Dextran-based polyelectrolyte multilayers: Effect of charge density on film build-up and morphology

Aurore Delvart, Céline Moreau, Angélina D'orlando, Xavier Falourd, Bernard Cathala

# Dextran-based polyelectrolyte multilayers: effect of charge density on film build-up and morphology.

*Aurore Delvart [a,*], Céline Moreau [a], Angélina D'Orlando [b], Xavier Falourd [b] and Bernard Cathala [a].*

[a] INRAE, UR1268 BIA, F-44316, Nantes, France

[b] INRAE, BIBS facility, F-44316 Nantes, France

Aurore Delvart: aurore.delvart@inrae.fr

Céline Moreau: celine.moreau@inrae.fr

Angélina D'Orlando: angelina.dorlando@inrae.fr

Xavier Falourd: xavier.falourd@inrae.fr

Bernard Cathala: bernard.cathala@inrae.fr

**\*Corresponding author**

INRAE Centre Pays de la Loire BIA 1268

3 impasse Yvette Gauchois

La Géraudière – CS 71627

44316 Nantes Cedex 3

*E-mail: aurore.delvart@inrae.fr (Aurore Delvart)

ABSTRACT

We have studied the growth process of thin polyelectrolyte (PE) films fabricated by the layer-by-layer assembly (LbL) and composed of Dextran sulfate with high (DexS H) and low (DexS L) sulfation rate and poly(allylamine hydrochloride) (PAH). Film growths were monitored by combining Quartz Crystal Microbalance with Dissipation monitoring (QCM-D), Surface Plasmon Resonance (SPR) and Atomic Force Microscopy (AFM). Even though, the two films growth up to 10 bilayers, QCM-D showed that polyelectrolyte pairs do not display similar behaviours. (PAH/DexS H) systems lead to linear growth, *i.e.* amounts deposited increase both for PAH and DexS H, while the PAH/DexS L pair generated zig-zag shaped asymmetric growth. Film water contents were determined by QCM-D solvent exchange and SPR experiments. DexS L contains less water than DexS H and in agreement with the QCM-D dissipation values that suggest the formation of more rigid films in the case of DexS L than DexS H. Surface morphology investigated by AFM display distinct surface patterns since DexS H form thin films with fibril-like morphology covering all the surface while heterogeneous films with "puddle-like" aggregates were imaged in the case of DexS L. Difference of charge compensation and charge neutralisation between both systems likely lead to dissimilar growth mechanisms that are tentatively proposed in this paper.

ABBREVIATIONS

PAH, poly(allylamine hydrochloride); DexS H, dextran sulfate sodium salt MW 40 kDa high sulfate content; DexS L, dextran sulfate sodium salt MW 40 kDa low sulfate content; $(PAH/DexS)_n$ multilayer, film with n bilayers of PAH and DexS.

INTRODUCTION

Dextrans are a family of α-glucans naturally produced by bacteria, whose main chain consists of D-glucose units linked by α-(1→6) type glycosidic bonds and which presents backbone with various size and ramifications, depending on the bacterium involved during production.[1] Within the increasing interest in the elaboration for biobased materials, dextrans present many interests such as their wide availability and their diversified structure differing in branching patterns or molar mass, but also with their functionalization ability due to the occurrence of hydroxyl groups on the surface of dextran main chain and branches.[2,3] Dextrans, partially degraded-dextrans and dextran derivatives find numerous applications in various areas as for instance in biomedical field, food science, cosmetics formulation and environmental field.[4–7] Low molecular weight dextrans can be used as a therapeutic agent for replacing moderate blood losses as blood-plasma substitute, as well as improving blood flow as blood volume expander.[8,9] Dextran polymers and derivatives have also be used in treatment involving the supply of iron in anaemic patients and as antiviral agent selective of various viruses.[10–12] They are great candidates for formulation of skin products and for food transformations, as they can be used as emulsifier, thickening agent and moistening agent.[13,14] Moreover, dextran derivatives provide a large range of charged or neutral polymers with different structures which present potential uses in chemistry and in environmental chemistry.[15,16]

Charged modified dextrans, such as dextran sulfates, have also been used for coatings and thin films elaboration. Their charged groups promotes interactions with other polyelectrolytes (PEs) and thus, their inclusion in polymers assemblies such as polyelectrolyte multilayers (PEMs).[17–20] Due to their availability and biocompatibility, dextrans have been already successfully incorporated in PEMs with various positively charged PEs for biological and biomedical applications. Among them, dextran sulfates are the most common ones integrated in PEMs formation : alternating pro- and anti-coagulant films,[21] antimicrobial and antifouling multi-

layered coating[22] or high loading efficiency systems and immobilization of biomacromolecules for drug delivey.[23]

Films of PEs can be typically formed using layer-by-layer (LbL) technique, introduced by Decher *et al.* in the 1990,[24,25] based on the alternative adsorption of cationic and anionic charged PEs, *via* the contribution of various driving forces.[35] Among all interactions, electrostatics between oppositely charged PEs was thought to be solely the main driving force for multilayer,[24] and the film build-up is explained by charge density of the adsorbing PEs and associated charge matching between poly-ions.[26,27] Schlenoff *et al.* have relayed studies on charge balance in PEMs based on the charge overcompensation and distribution in films and suggested a modelling method to determine growth mechanism of PEMs.[28,29] They discussed the amount of individual polymer as well as salt content and charges within individual layers and demonstrated the impact of charge overcompensation on the growth of layers. Furthermore, the authors suggest that polymer charges are responsible of intrinsic compensation while salt counterions are responsible of extrinsic compensation. However, defining a precise critical level of charge is not obvious since multilayer growth have been obtained with very low charged group amounts[30] and several works reveal the contribution of other driving non-electrostatic forces, such as hydrophobic forces or hydrogen bonds, especially when polysaccharides are involved.[30–32] Linear growth of the film thickness with the number of deposited layers is commonly obtained with strong PEs leading to stable PEMs. On the other hand, PEMs constructed from weakly charged PEs, polysaccharides or polypeptides are often characterized by a non-linear growth processes, due to the fast diffusion of both PE types into PEM films.[33–36] In fact, the internal structure of the PEM is governed by several parameters such as the degree of charge of the polyelectrolyte,[26] the pair of polyelectrolytes,[37,38] the ionic strength, the type of salts,[39] and the pH of the solution. Charge density can be tuned either by varying the pH in the case of weak polyelectrolytes or by adjusting the polymer structure in the case of strong charged moieties. In both cases, evaluation of the charge

density of the films structure and properties represent a challenging investigation as well as real opportunity to tune and control the thin films structure. Moreover, LbL assemblies generally entrap significant amount of water[40] and swelling/deswelling character of PEMs can be controlled by : modulation of PEs chain conformation in solution or introduction of hydrophobicity in the system[41,42] by selecting counterion,[43] decreasing the ionic strength[44] or reducing the poly-ions charge density.[45] In 2012, Kittle *et al.* demonstrated that water content of nanocomposites based on various dextrans can be modified by changing the degree of substitution and the hydrophobic content of absorbed charged dextrans derivatives.[41]

In the present study, we report the investigation of PEMs growth containing Poly(allylamine hydrochloride) (PAH) and Dextran Sulfates (DexS) with different charge densities determined by ^{1}H NMR. We investigate the films growth mode by Quartz Crystal Microbalance with Dissipation Monitoring (QCM-D) and Surface Plasmon Resonance (SPR), with special focus on the water content. Those two techniques permit quantitative, real-time, in situ, non-invasive and highly sensitive detection and determination of the adsorbed molecules on various type of surfaces, including biopolymers and polysaccharides.[46–48] By accessing the variation of the shear rate of an oscillating piezoelectric sensor, QCM-D probes variations in total mass and viscoelastic properties of the absorbed species coupled with solvent i.e. the "wet" film formed on a surface. SPR allows to determine the "dry" mass of the adsorbed film from change of refractivity of the surface caused by the adsorption of molecules. A combination of those methods supplies significant information of the layer-by-layer adsorption mechanism, structural changes and the extent of hydration. The morphologies of the layer were investigated with Atomic Force Microscopy (AFM). In this work, we describe how charge density of DexS affects film growth and morphology of (PAH/DexS) PEMs. These experimental investigations should lead to a better understanding of the construction of PEMs based on dextrans derivates as well as allow to control the surface patterning of films by variation of the dextran charge content.

EXPERIMENTAL SECTION

**Materials.** Poly(allylamine hydrochloride) (PAH) with a molecular mass in the range of 120 – 200 000 g.mol$^{-1}$ was purchased from Polysciences (Germany) and was used as a polycation. Dextran sulfates (M$_W$ ~40 000 g.mol$^{-1}$) obtained from Sigma Aldrich (Germany), one noted as high sulfate content (DexS H) and the another one as low sulfate content (DexS L), were employed as polyanions. Chemical structures of DexS are described on Figure 1a. All polymers were dissolved in deionized water (18.2 m$\Omega$, Millipore Milli-Q purification system) containing 25 mM NaCl at 0.1 g.L$^{-1}$ for PAH and at 0.5 g.L$^{-1}$ for DexS during 12 hours at room temperature under agitation. All solutions were stocked at 4°C. The pH of PAH solution and both DexS solutions was measured between pH 6 – 6.5. Deuterium oxide D$_2$O (98%) used for D$_2$O/H$_2$O exchange was purchased from Euriso-Top (France).

**Characterization of Dextran Sulfate**

Molar masses were determined using High-Performance Size-Exclusion Chromatography (HPSEC) with OMNISEC Reveal and OMNISEC Resolve (Malvern Panalytical Ltd., Malvern, UK). DexS were dissolved at 5 g.L$^{-1}$ in deionized water (18.2 m$\Omega$, Millipore Milli-Q purification system) and filtrated at 0.45 μm before measurement. The DexS samples were eluted at a range of 0.7 mL/min with 50mM NaNO$_3$ containing 0.02% NaN$_3$. The column used was a polymethyl-methacrylate (A-series) A5000 column (300 mm x 7.8 mm) and intrinsic viscosity determinations were performed using a viscometer included in multi angle light scattering detector Viscotek SEC-MALS 9 (Malvern Panalytical Ltd., Malvern, UK). Intrinsic viscosity data were recorded using OMNISEC 11.01 software (Malvern Panalytical Ltd., Malvern, UK). Molar masses were obtained using Mark-Houwink equation:

(1)     $[\eta] = K \times M_v{}^{\alpha}$

where *[η]* (dL.g$^{-1}$) is intrinsic viscosity obtained with HPSEC, $M_v$ (g.mol$^{-1}$) is the polymer viscosity-average molar mass and *K* (dL.g$^{-1}$)*, α* are viscosity-molecular weight constants for particular polymer-solvent combination. Values of *K* and *α* were assumed to be respectively 7.337×10$^{-4}$ dL.g$^{-1}$ and 0.533 according to value for dextrans at 20°C reported by Güner.[49]

Molar masses obtained were consistent with supplier data.

[1]H nuclear magnetic resonance (NMR) experiments were carried out on a Bruker AvanceIII 400 NB spectrometer operating for ^{1}H, equipped with a double-resonance H/X BBo 5-mm probe. Between 90 and 95 mg of dextran sulfates were solubilized in 1 g of 99.96% $D_2O$. All spectra were recorded at 30°C using a [1]H 90° pulse of 10.2 µs and 128 accumulation with a recycle delay of 10 s. Acquisitions parameters including a water signal pre-saturation applied to decrease the HDO signal in the same order of magnitude than the others peaks. NMR spectra deconvolution was performed using the PeakFit® software (Systat Software, Inc., US). Peak chemical shifts and relative contribution were assigned according to the study report by Neville *et al.*[50]

**(PAH/DexS) film deposition by dipping method.** Multilayer films were deposited on silicon wafers as solid substrates for AFM analysis. Surfaces were cleaned in piranha bath (mixture of $H_2O_2/H_2SO_4$ at 70%/30% v/v) for 30 minutes for silicon wafers, then they were extensively rinsed in pure deionised water and dried under a $N_2$ stream. (PAH/DexS) multilayer films were also formed by LbL method using dipping procedure. Silicon substrates were alternately immersed in PAH solution and DexS solution for 5 minutes. Between each adsorption step, the surfaces were rinsed in 3 water baths containing no NaCl. The dipping sequence was repeated n times to form (PAH/DexS)$_n$ with n the number of bilayers on the substrate where a (PAH/DexS) bilayer (n = 2) is a double layer composed for a single PAH layer and a single DexS layer. All surfaces were dried under $N_2$ stream once 10 bilayers, (PAH/DexS)$_{10}$, were assembled.

**Quartz Crystal Microbalance with Dissipation Monitoring (QCM-D).** A QCM-D equipment (E4 Q-Sense instrument, AB, Sweden) was used to investigated the adsorption process of PAH

and DexS in the formation of (PAH/DexS) PEMs. Films were deposited on gold-coated quartz crystals (QSX301, Q-Sense) which were cleaned in piranha bath for 5 minutes. The quartz crystals used, AT-cut quartz crystal coated with a nominal resonance frequency of 5 MHz ($f_0$), were introduced into the cell and water was introduced at a flow rate of 50 µL.min$^{-1}$ at 20°C for at least 1 hour until a stable baseline was obtained. First, PAH solution was injected at the same flow rate for 5 minutes, followed by 5 minutes of water rinsing. Then DexS solution was injected at 50 µL.min$^{-1}$ for 5 minutes, once again followed a 5-minutes rinsing step. The variations in frequency ($\Delta f$) and dissipation ($\Delta D$) signals were recorded at the fundamental resonance frequency and its overtones (from 3$^{rd}$ overtone to 7$^{th}$ overtone). All experiments were repeated at least 3 times.

Normalized shifts in frequency ($\Delta f_n/n$) due to additional mass on the sensor surface can be linked to the adsorbed mass ($\Delta m$) using Sauerbrey equation for rigid films (dissipation $\Delta D_n/n < 1 \times 10^{-6}$) or using viscoelastic modeling for non-rigid films (dissipation $\Delta D_n/n > 1 \times 10^{-6}$).[51,52]

In this study, the interpretation was done with Dfind Smartfit model on QSense Dfind® Software (version 1.2.6, Biolin Scientific, Q-Sense, Sweden), which integrates both frequency and dissipation assuming a film density $\rho$ of 1.200 g.cm$^{-3}$ for all films.[17,53] The film built under LbL process was assumed to have a uniform thickness and a uniform density. The model, based on Kelvin-Voigt model, was fitted with at least four overtones with a good signal-to-noise S/N ratio and gave access to film thickness, shear elastic modulus and shear viscosity.[42] Only values from fit with quality indicator higher than 0.70 were used. The adsorbed mass $\Gamma_{QCM-D}$ (ng.cm$^{-2}$) of the polymer layer in hydrated state was calculated as follows:

(2) $\qquad \Gamma_{QCM-D} = d_{QCM-D} \cdot \rho$

where $d_{QCM-D}$ is the film thickness obtained with QCM-D technique (nm) and $\rho$ (g.cm$^{-3}$) is the assumed density of the film.

**Surface Plasmon Resonance Measurement (SPR).** Building of (PAH/DexS) PEMs was followed by SPR on a Biacore ×100 instrument (Sweden) using gold-coated chips (SIA kit Au,

GE Healthcare, France) cleaned in piranha bath for 5 minutes. The sensor was slide into the equipment flow cell, where desionised water was injected at a flow rate of 30 μL.min$^{-1}$ at 20°C until baseline stabilization. Then PAH solution and DexS solution was alternately introduced for 5 minutes, followed by 5-minutes injection of deionized water at 30 μL.min$^{-1}$ flow rate.

SPR measurements reports changes in the refractive index (n) of a surface, caused by the adsorption of molecules on it. A change in the refractive index induces a variation in the SPR angle $\Delta\theta$, which is detected by SPR equipment.[41,42,54] The SPR angle is related to the thickness and mass concentration of the absorbed layers without associated water and the thickness $d_{SPR}$ (nm) was determined using the following equation derivatized from Feijter et al. equation:[55]

(3) $\qquad d_{SPR} = \frac{l_d}{2} \frac{\Delta\theta}{m(n_a - n_s)}$

where $l_d$ is a characteristic decay length of the evanescent electromagnetic field estimated at 0.37 of the light wavelength ($\lambda_d$ = 281.2 nm), $m$ is a sensitivity factor for the sensor obtained after calibration of the SPR (101.93°/RI), $n_s$ is the refractive index of the bulk solution ($n_s$ = 1.33371), $n_a$ is the refractive index of the adsorbed species in rigid and compact film. In this study, the refractive index $n_a$ was assumed to be 1.49 and 1.48 respectively for PAH and DexS, which are values for rigid dry films entirely made of the polymer. The adsorbed mass $\Gamma_{SPR}$ (ng.cm$^{-2}$) was calculated as follows:

(4) $\qquad \Gamma_{SPR} = d_{SPR} \cdot \rho$

where $d_{SPR}$ is the film thickness (nm) and $\rho$ is the density of the film.

**Determination of Water Content of films.** Calculated QCM-D mass $\Gamma_{QCM-D}$ represents the hydrated layers, *i.e.* the absorbed polymer and the coupled water while calculated SPR mass $\Gamma_{SPR}$ is related to the "dry" mass, *i.e.* the polymer without water.[46,47] Using both techniques, the water content of (PAH/DexS) films, H$_2$O$_{SPR/QCM}$ (%) is calculated as follow:

(5) $\qquad H_2O_{SPR/QCM}(\%) = \frac{\Gamma_{QCM-D} - \Gamma_{SPR}}{\Gamma_{QCM-D}} \times 100\%$

9

The water content by switching the solvent from water to deuterium oxide $D_2O$ was calculated using QCM-D.[41,56,57] The *$H_2O/D_2O$* solvent exchange was performed with one (PAH/DexS) bilayer constructed in the same conditions as described in the section "QCM-D". After stabilization in $H_2O$ at a flow rate of 50 µl.min$^{-1}$, $D_2O$ is injected for 5 minutes followed by rinsing with $H_2O$ during 30 minutes. The same experiment was done using the bare quartz substrate as reference system.

The changes in frequency between bare quartz crystal *$(\Delta f_n/n)_{bare}$* and quartz crystals covered by layers *$(\Delta f_n/n)_{film}$* allow to determine the frequency shift $(\Delta f_n/n)_{water}$ caused by solvent exchange with the following equation:[41,56]

$$(6) \quad \left(\frac{\Delta f}{n}\right)_{water} = \frac{\left(\frac{\Delta f}{n}\right)_{film} - \left(\frac{\Delta f}{n}\right)_{bare}}{\left(\frac{\rho_{D2O}}{\rho_{H2O}}\right) - 1}$$

where *n* the overtone number and *ρ* the densities of solvent, 0.998 g.cm$^{-3}$ for $H_2O$ and 1.106 c.cm$^{-3}$ for $D_2O$ at 20°C. The water content from $H_2O/D_2O$ exchange, $H_2O_{exchange}$ (%), can then calculated as:

$$(7) \quad H_2O_{exchange}(\%) = \frac{\left(\frac{\Delta f}{n}\right)_{film}}{\left(\frac{\Delta f}{n}\right)_{water}} \times 100\%$$

**Atomic Force Microscopy Measurement (AFM).** AFM images (height, error-signal and phase images) of multilayered films absorbed on silicon wafers were recorded in air employing INNOVA AFM from Bruker (France). Images were registered with low scan rates (0.3 Hz) using nitride coated silicon probes whose spring constants are 37 N.m$^{-1}$ (TESPA-VS, Bruker, France). All images were taken at both 10 µm × 10 µm and 5 µm × 5 µm at a resolution of 512 × 512 points. Treatment to improve AFM images and their analysis were done using Gwyddion Software (version 2.58, developed by Czech Metrology Institute). Based on three AFM images per surface, the surface root mean squared (RMS) roughness was quantified. In addition of RMS, scratching

method were realized to obtain average height and height profiles by analysis eight zones of a surface scratched with a razor blade.
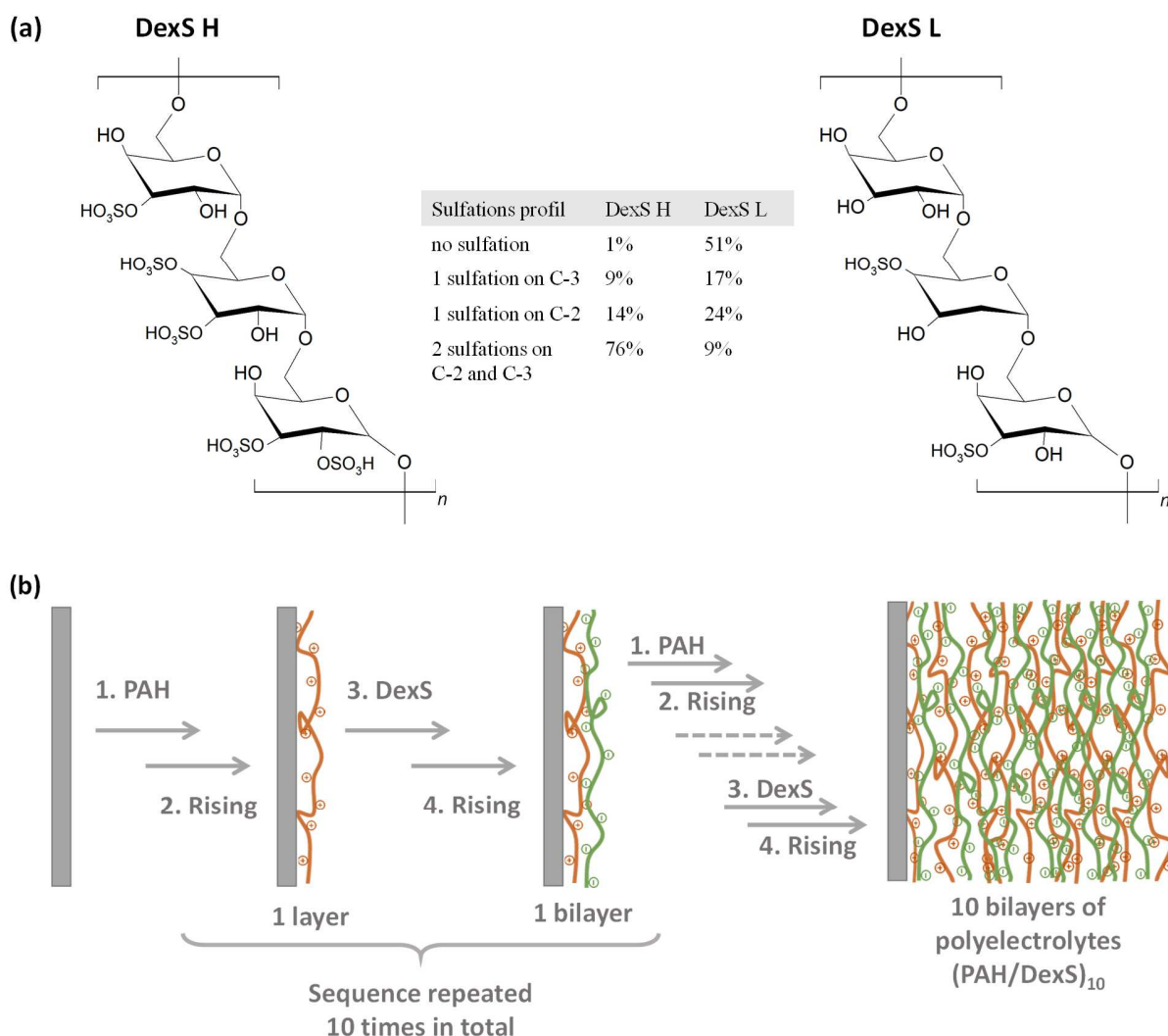
RESULTS AND DISCUSSION



**Figure 1.** (a) Chemical structures of dextran sulfate with high sulfate content DexS H (at left) and low sulfate content DexS L (at right); sulfation patterns of both DexS are indicated. (b) Demonstrative scheme of the LbL formation of films from cationic PAH (orange chains), and negatively charged DexS (green chains) in solid substrate (grey bar).

**Fabrication of the LbL films.** We focused on poly(allylamine hydrochloride) (PAH) as polycation and two dextran sulfates (DexS) as polyanions since this polyion pair has demonstrated its ability to build LbL films as well as layered nanocapsules.[58,59] Figure 1a presents the structure of the dextran sulfate used in this study. DexS have the same molar mass and the same

D-glucose backbone linked by α(1→6) glycosidic linkages (Figure 1a). They differ only by their charge densities and sulfate substitution patterns as determined by ^{1}H NMR (Table in Figure 1a and Figure S1). DexS with high sulfate content (DexS H) is mainly disubstituted since NMR spectra displays peaks for simultaneous sulfation at C-2/C-3 (76%) and -or monosubstituted either at C-2 or C-3 (14 and 9 %, respectively). On the contrary, DexS with low sulfate content (DexS L) shows peaks for monosulfation at C2 and C3 (24 and 17%) and little amount of disulfation (9%) (Supporting Information, Figure S1). A majority of unsulfated glucose units were also detected (51%) for DexS L. In summary, all glucose units of DexS H bear at least on charge, a majority being double charged leading to an average charge density of 1.75 charges per glucose unit, while, in the case of DexS L, only 0.6 glucose groups in average are charged. In the case of poly(allylamine hydrochloride) (PAH), the polymer contains 1 amino group by monomer unit taking into account the neutral pH of the polymer solution so that all the amino groups are charged leading to the presence of 1 charge per monomer. This estimation gives a rough overview of potential electrostatic interaction between DexS and PAH since other parameters such as the molar mass of the monomers, the stiffness of the chains and the chains conformation will also influence the polymer adsorption. Nevertheless, the difference of charge density between the two DexS is significant and relevant to explain their adsorption behaviours.

Adsorptions of PEs solutions were monitored by QCM-D and carried out in 25 mM NaCl followed by a rinsing step in pure water to remove all loosely bound polymers or salt excess as in classical LbL process (Figure 1b). These conditions are in agreement with previous studies on salt concentration effect, as it is well known that salt can affect the thickness, surface roughness and the structure of the films.[60–63] For similar films with PAH, NaCl concentration used is between 10 mM NaCl and 1 M NaCl.[60–63]. Polymer concentrations can also influence the multilayer film assembly and its adsorption kinetics; PAH concentration (0.1 g.L$^{-1}$) and DexS concentration

(0.5 g.L$^{-1}$) were chosen according to our previous studies one QCM-D monitored LbL growth.[37,61]
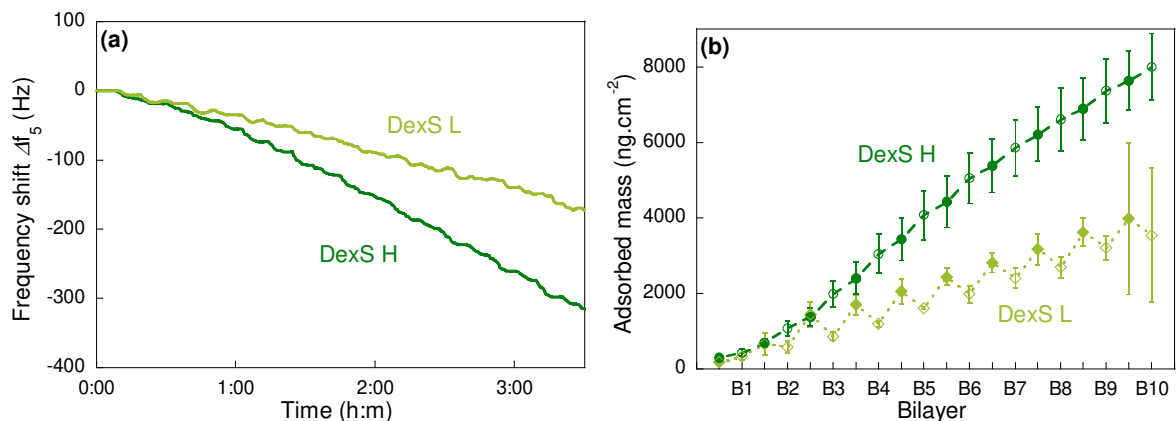


**Figure 2.** (a) Graph of $\Delta f_5$ vs time for (PAH/DexS)$_{10}$ multilayer with DexS H (dark green) and DexS L (light green) building on gold coated surface. (b) Adsorbed mass evaluated with Voigt model for (PAH/DexS)$_{10}$ multilayer with DexS H (dark green) and DexS L (light green). Bn corresponds to the n$^{th}$ (PAH/DexS) bilayer of the multilayer, the full symbols are representatives of PAH adsorption while the open symbols are representatives of the DexS adsorption.

The successful growth of (PAH/DexS)$_{10}$ PEMs on gold surface is demonstrated by QCM-D traces shown in Figure 2a. A decrease of frequency at each layer deposition is observed for both DexS indicating of PE adsorption. In addition, the formation of stable PEMs is observed as frequency signal remains constant after the rinsing step. Different $\Delta f$ values after 10 bilayers due to hydrated mass deposition were observed indicating different adsorption behaviour. The mass absorbed at each step during the film process is given using the Voigt model for viscoelastic films and values are reported in Figure 2b.[54] Films based on DexS H result in a final frequency shift of -320 Hz for a total mass absorbed of about 8000 ± 870 ng.cm$^{-2}$ while films based on DexS L result in a final frequency shift of -165 Hz for a total mass absorbed of 3600 ± 1770 ng.cm$^{-2}$ for 10 bilayers. For both dextran two regimes were observed (Figure 1b). The first one between bilayer 1 and bilayer 3 and a second one after bilayer 3, as previously observed for others systems during

multilayer assembly.[64,65] The first one, *i.e.* before the bilayer 3, is mainly driven by the substrate surface properties while the second one is related to the formation of a surface charge excess only related to bilayer structure. Thus the adsorption behaviour of the PE couple (PAH/DexS) becomes independent from the surface chemistry of the substrate.[64,66] In the case of DexS H, the second regime highlights also a linear growth with an average mass increase of 858 ng.cm$^{-2}$ per bilayer. Whatever the PE deposited, PAH or DexS H, the adsorbed mass increases. However, it may be noted that PAH deposition yields to lower value (338 ng.cm$^{-2}$) while DexS H deposition yields to higher value (520 ng.cm$^{-2}$). The amount being evaluate by QCM-D, associated water must be also considered, and will be discussed after. The (PAH/DexS L)$_{10}$ PEMs also exhibited a linear regime after bilayer 3 based with, however, a lower average mass increment of 375 ng.cm$^{-2}$ for bilayer deposition in average. Remarkably, the growth pattern displays non-monotonous zig-zag shaped growth (Figure 1b). PAH layer adsorption on DexS L layer presents an increase of average mass deposition of 835 ng.cm$^{-2}$ while adsorption of DexS L layer on PAH layer displays an average mass loss of 460 ng.cm$^{-2}$. This behaviour has been already observed and was associated to an adsorption-desorption process of hydrated polymers that can either removed from the surface due to loose attachment or expulsion of water and/or counter-ions from the film.[67,68] Moreover, even though both PEs allow to build stable films, they display different adsorption behaviours (symetric linear growth vs asymmetric linear growth) as well as a higher amount of polymer adsorbed for (PAH/DexS H)$_{10}$ films.
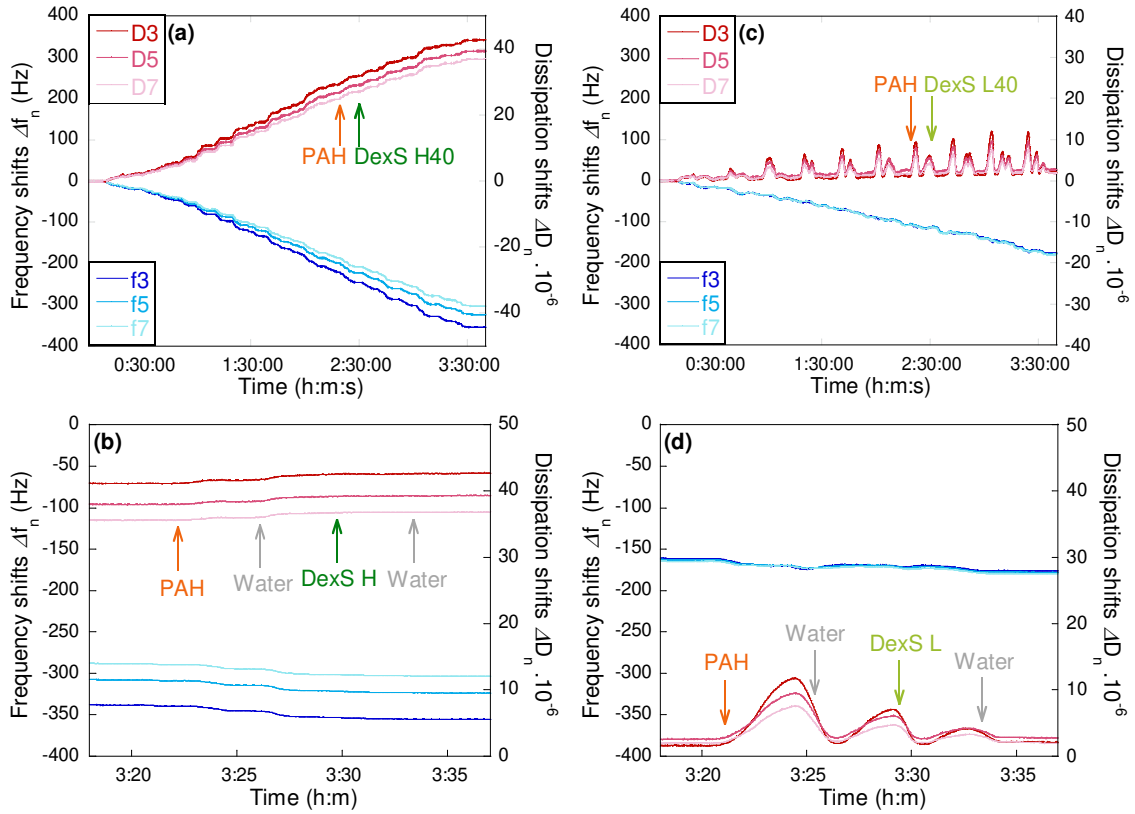
**Figure 3.** (a), (c) $\Delta f_n$ and $\Delta D_n$ as function of time for (PAH/DexS)10 multilayer on gold coated quartz crystal using QCM-D. The frequency (blue) and dissipation (red) changes for the third, fifth and seventh overtone are depicted. (b), (d) Zoom on the bilayer 10 build-up with adsorption of PAH (orange), rising with pure water (grey), adsorption of DexS (green).

**Viscoelastic behaviour and water content of the films.** To investigate (PAH/DexS H) and (PAH/DexS L) films building mechanisms, QCM-D frequency and dissipation shifts were analysed deeply. The frequency shifts of both (PAH/DexS H)$_{10}$ and (PAH/DexS L)$_{10}$ assemblies are displayed for the third, fifth and seventh overtones on Figure 3a,c. Qualitatively, the comparison between the different overtones of frequencies and dissipation signals gives information on structural and viscoelasticity properties of the adsorbed film. As observed in Figure 3a, a splitting of frequencies for (PAH/DexS H) is observed during the 10 bilayers build-up. (PAH/DexS L) PEMs do not behave similarly since the frequencies are almost superimposable (Figure c). Expanding closer on the formation of the bilayer 10 (Figure 3b,d) confirms the absence

16

of splitting between frequencies for films based on DexS L while a difference of 50 Hz between the 3rd and the 7th overtones is observed. In addition, as illustrated on Figure 3b and 3d, (PAH/DexS H) films present an average final dissipation of $30\times10^{-6}$ while (PAH/DexS L) PEMs display an average final dissipation of $2\times10^{-6}$, respectively. This indicates different viscoelastic properties with a more rigid film for (PAH/DExS L) as compared to (PAH/DexS H) film. These properties can be qualitatively compared through the $-\Delta D/\Delta f$ ratio calculated from final frequencies and dissipation values reported on Figure 3b,d since the ratio correspond to a normalization of dissipation variation per unit of mass adsorbed.[69,70] Final ratio $-\Delta D_5/\Delta f_5$ (after rising of bilayer 10) for (PAH/DexS L) films is an order of magnitude lower ($0.015\times10^{-6}$ $Hz^{-1}$) than (PAH/DexS H) value ($0.122\times10^{-6}$ $Hz^{-1}$) which confirms that the PAH/DexS L film is more rigid than the PAH/DexS H. From literature, value of about $0.3\times10^{-6}$ $Hz^{-1}$ have been measured for poly(acrylic acid)/poly-L-lysine pairs[70] and values varying from 0.1 to $0.5\times10^{-6}$ $Hz^{-1}$ have been found for PEMs based on cellulose nanocrystals/hemicellulose, *i.e.* non-electrostatic based systems.[69] This clearly indicates that (PAH/DexS) PEMs are quite rigid and especially (PAH/DexS L) systems after DexS L adsorption step.
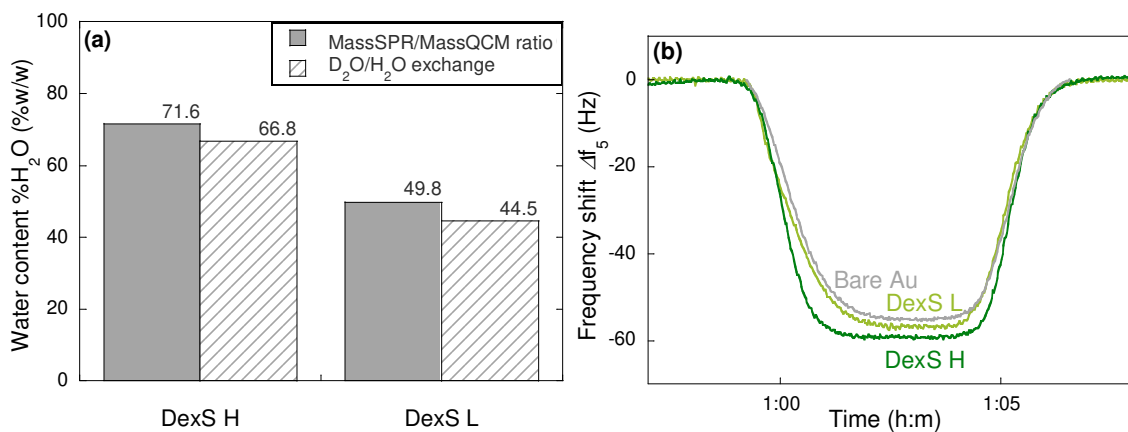


**Figure 4.** (a) Water content (%w/w) of the films calculated from the ratio of adsorbed mass obtained by SPR and adsorbed mass obtained by QCM-D on the 2nd bilayer and the value calculated from $D_2O$-$H_2O$ exchange on the 2nd bilayer. (b) $\Delta f5$ vs time for $D_2O$-$H_2O$ exchange on

the $2^{nd}$ bilayer of (PAH/DexS H) multilayer (dark green) and of (PAH/DexS L) multilayer (light green).

Besides information provided by QCM-D on hydrated absorbed mass on substrate, SPR allows to calculate a "dry" polymer mass, i.e. the mass of polymer contained in the films without the contribution of the water bound. From equation (4) and equation (5), SPR absorbed masses are determinate to be 130 ng.cm$^{-2}$ for (PAH/DexS H)$_2$ PEMs and 120 ng.cm$^{-2}$ for (PAH/DexS L)$_2$ PEMs. Meanwhile, hydrated masses from QCM-D are 1100 ng.cm$^{-2}$ for (PAH/DexS H)$_2$ PEMs and 570 ng.cm$^{-2}$ (PAH/DexS H)$_2$ PEMs, which suggest that (PAH/DexS H)$_2$ films contain more water than (PAH/DexS L)$_2$. Based on QCM-D and SPR data, water content $H_2O_{SPR/QCM}(\%)$ was found to be about 72% in the case of DexS H and 50% in the case of DexS L (Figure 4a).

Water content has also be evaluated from $H_2O/D_2O$ exchange experiment as monitored by QCM-D, i.e. $H_2O_{exchange}(\%)$.[56] Figure 4b shows the change in frequency ($\Delta fn/n$) versus time for the (PAH/DexS)$_2$ PEMs switched from $H_2O$ to $D_2O$ and back to $H_2O$. The calculated water content of films was lower for (PAH/DexS L) films (44.5 %) than for the (PAH/DexS H) films (66.8%). Both analyses give consistent values of water content around 66 – 72% of water for (PAH/DexS H)$_2$ PEMs and 44 – 50% of water for (PAH/DexS L)$_2$ PEMs (Figure 4b). As discussed in the previous section, PEMs build from DexS H are more hydrated than PEMs build from DexS L consistent with a less rigid film structure.

**Surface Morphology and Roughness.** AFM was performed to analyse the surface morphology and roughness of the (PAH/DexS) adsorbed layers on the silicon wafer after adsorption, in a dry state, and images are reported on Figure 5. After drying of 5 (PAH/DexS) and 10 (PAH/DexS) adsorbed bilayers, different patterns are observed on both films as illustrated on Figure 5. (PAH/DexS H) PEMs exhibit a surface displaying fibrillar network pattern while (PAH/DexS L) PEMs present a more granular surface with "puddle-like" aggregates. Similar aggregates in the

dry state were previously observed for various porous PEMs based on synthetic and natural polymers[34,36,71,72], proteins and complex of biopolymers and proteins[46,73] and well-known microporous surfaces [74,75]. For both dextran sulfate, increasing the number of bilayers seems to lead to a better surface coverage, as AFM images for PAH10 and DexS10 shows lower contrast than images for PAH5 and DexS5. Moreover, in the case of (PAH/DexS L), surface morphology seems to changes between PAH adsorption step and DexS adsorption step. Images on PAH10 show better surface coverage than images on DexS10, *i.e.* adsorption of DexS10 on PAH10 seems to reduce covered surface.
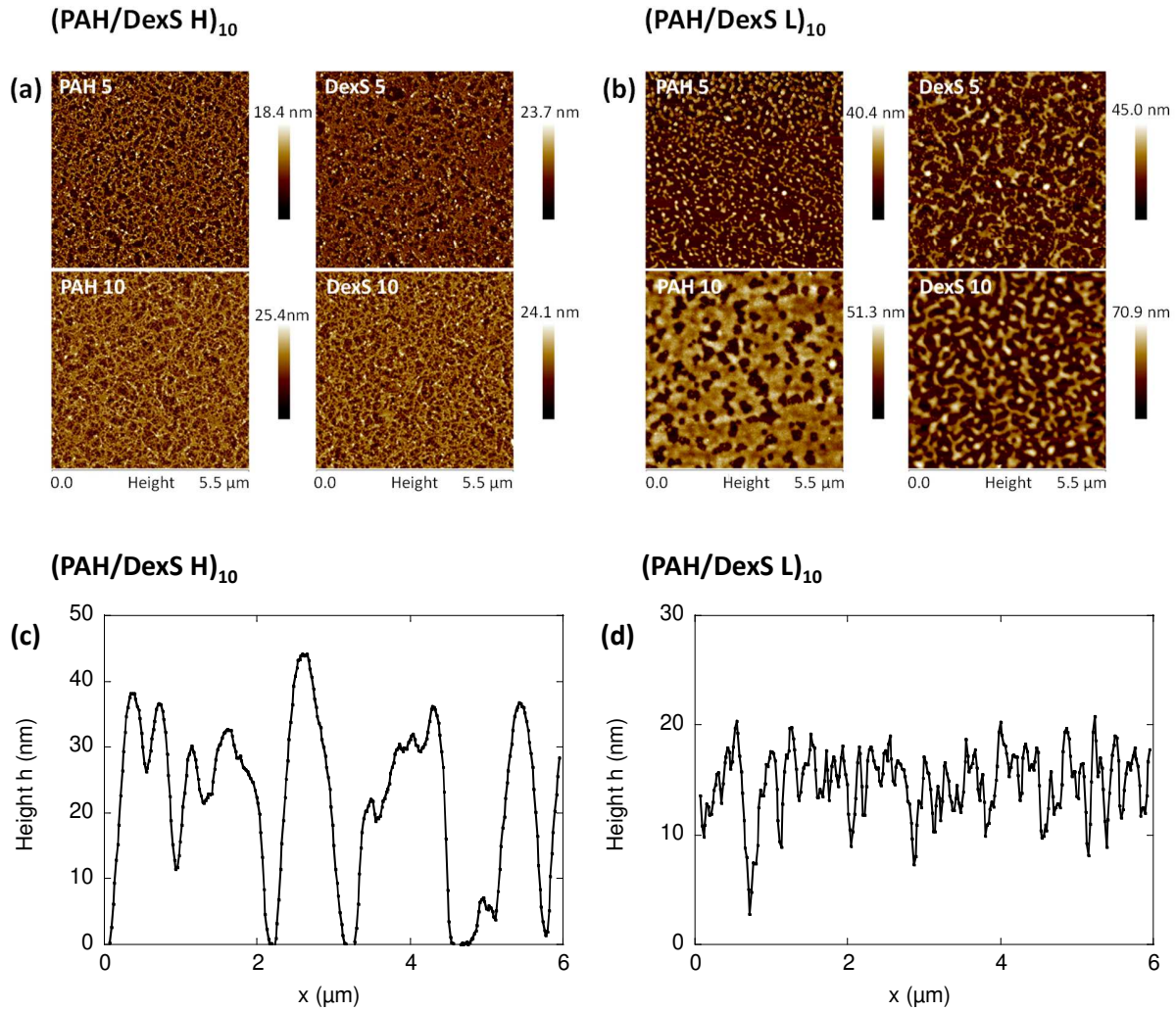


**Figure 5.** AFM topography images from (a) (PAH/DexS H) multilayer and (b) (PAH/DexS L) multilayer of (on the top) the PAH 5 (bilayer 4.5 *i.e.* outermost layer of PAH before bilayer 5), the

DexS 5 (bilayer 5), and of (on the bottom) PAH 10 (bilayer 9.5 *i.e.* outermost layer of PAH before bilayer 10) and DexS 10 (bilayer 10). Height profiles of (c) (PAH/DexS H)$_{10}$ and (d) (PAH/DexS L)$_{10}$ using AFM topography images on scratched surface.

Additionally, thicknesses of the layers were determined by AFM topography images of scratched dry layers and height profiles are presented in Supporting Information (Figure S2). Using the scratch method on the 10$^{th}$ bilayer, *i.e* DexS10 layers, height ranges and roughness of surfaces are obtained. (PAH/DexS H)$_{10}$ composites present a height of 15.01 nm ± 4.78 nm and a RMS roughness of 4.06 nm ± 0.79 nm. (PAH/DexS L) PEMs building lead to a thicker and a rougher surface; "puddle-like" aggregates of (PAH/DexS L)$_{10}$ present an average height of 19.87 nm ± 1.51 nm and an average RMS roughness of 24.49 nm ± 12.05 nm indicating a heterogeneous structure due to holes between aggregates. The film built based on DexS L presents a higher thickness after drying and a different surface morphology compared to film built with DexS H.

**(PAH/DexS) thin film formation.** Even though (PAH/DexS) systems present a similar linear growth up to 10 bilayers but different adsorption mechanisms leading to different adsorbed hydrated mass and film surface morphology have been revealed. As (PAH/DexS) systems present the same characteristics in terms of PEs chemical structure, their adsorption behaviour can be mainly attributed to their difference in charge density. Indeed, while DexS H (high sulfate content) displays 1.75 charges per monomer, DexS L (low sulfate content) displays 0.6 sulfate charges per monomer.

In the case of DexS H, (PAH/DexS H) system allowed to film growth linearly with increase of adsorbed amount of PEs at each adsorption step. QCM-D data, dissipation values and $-\Delta D_5/\Delta f_5$ ratio highlighted the fact that (PAH/DexS H) PEMs presented a viscoelastic behaviour in agreement with higher water content (~69%) than (PAH/DexS L)$_{10}$ systems that lead to a quite rigid film as evidenced by the lower $-\Delta D_5/\Delta f_5$ ratio and water amount as compared to (PAH/DexS

H) PEMs (~47%). Interestingly, (PAH/DexS L) PEMs present an asymmetric growth between polycation and polyanion adsorption with high hydrated mass adsorbed from PAH while a mass loss is observed for DexS L adsorption. In addition, DexS H or DexS L surface morphology of films obtained after drying investigated by AFM presents also dissimilarities. (PAH/DexS H) thin films display with fibril-like surface while (PAH/DexS L) PEMs leaded to rougher films forming "puddle-like" aggregates. Moreover, while (PAH/DexS H) PEMs present similar surface morphology with PAH or DexS ending, (PAH/DexS L) PEMs look like surface differ between PEMs ending with PAH and PEMs ending with DexS L. The morphology observed in AFM confirm the influence of charge density of DexS H and DexS L on film architecture, but also the impact of DexS L adsorption on the internal restructuration of (PAH/DexS L) PEMs. The specific surface pattern remind surface morphology previously observed for others systems and attributed to the formation of polyelectrolyte-complexes[76], that may indicate the complexation of PAH and DexS L onto the surface. This complexation can be due to charge neutralisation in the films and thus lead to water removal and an increases of hydrophobic content of the film as it was previously observed by Kittle *et al.*[41]

From all information collected in this study, Figure 6 presents tentative mechanisms of film building explaining differences observed in the two systems.
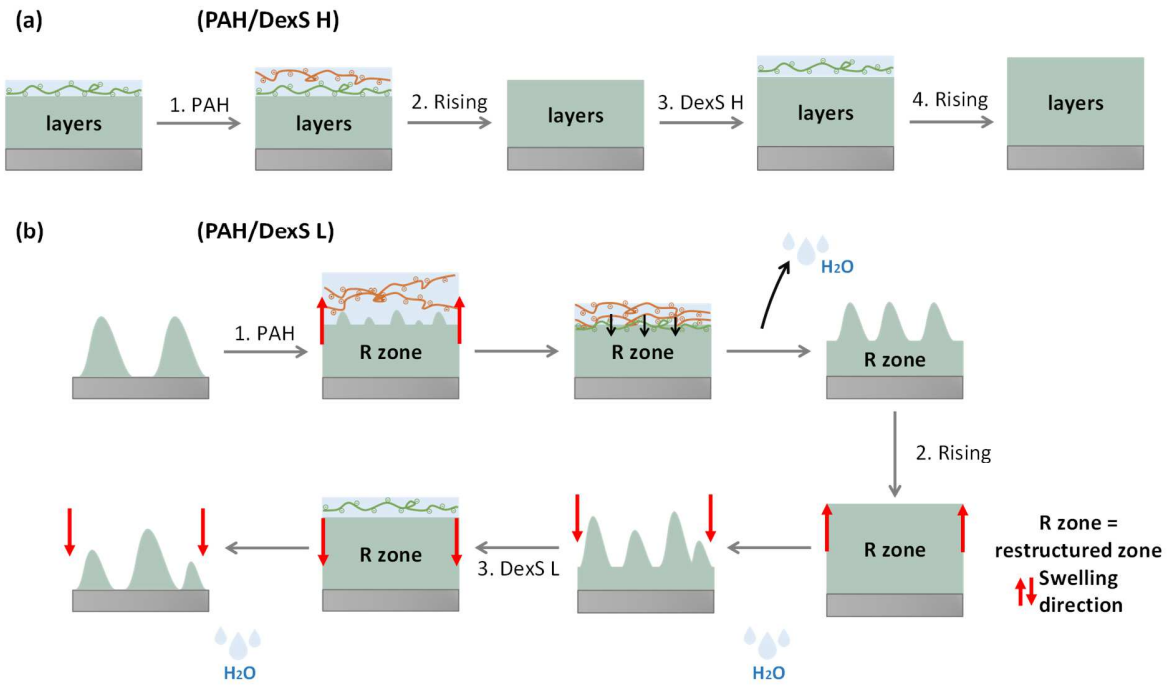
**Figure 6.** Proposed mechanisms for the build-up of (a) (PAH/DexS H) PEMs and (b) (PAH/DexS L) PEMs starting from bilayer 4 on PEMs previously ending with DexS.

In the case of (PAH/DexS H) films, illustrated on Figure 6a, the amount of negative charges from DexS H are likely high enough to largely overcompensate charges coming from previous PAH layer that might provide high surface charge density after DexS H adsorption (Figure 6a).[77] In the *Step 1,* the adsorption of PAH on adsorbed DexS layer leads to an increase in mass and in dissipation as hydrated PAH is adsorbed. During the *Step 2,* water rising does not seem to induce any mass loss which indicate that previous layers were charged enough to be strongly linked to the surface undernear. Thus, (PAH/DexS) system leads to the formation of stable and charged layers. Then, the adsorption of DexS H on previous PAH layer (*Step 3*) followed by the rinsing step (*Step 4*) leads to surface charge inversion and no significant DexS and counter-ion excess removing. During these four steps, the amount of water in the layer is stable and PE form stable and highly charged layers.

For (PAH/DexS L) systems (Figure 6b), the adsorption mechanism is more complex. At the *Step 1*, adsorption of PAH induces an increase of film hydration and a decrease of the film rigidity followed by an internal film restructuration. As DexS L presents a number of charges per monomer comparable to the number of charges presents on PAH monomer, a partial neutralisation of sub-layers with PE adsorption occurred, which contributes to the diffusion of the adsorbed PAH into the (PAH/DexS L) PEMs. During the rising in *Step 2*, the film swells again that may promote further diffusion internal and restructuration of PEMs. Charge neutralisation itself generates a water removal as shown by Kittle *et al.* (2012).[41] During *Step 3*, as soon as DexS L diffusion starts after adsorption, charge compensation between PAH and DexS L occurred inside the films that likely promote charge neutralisation then complexation between PAH and DexS L. Formation of PEs-complexes decreases electrostatic repulsion between PEs and the affinity with bonding-water of highly hydrated PAH/DexS decreases resulting in the water expulsion from the film. This film dehydration, also named deswelling or dewatering, favour short range interactions within the final system[42,56] and induce PAH/DexS L aggregation onto the surface leading to the "puddle-like" pattern (*Step 3*).[76]

CONCLUSIONS

Dextran sulfate (PAH/DexS) PEMs films with linear growth were successfully constructed and we demonstrated that difference of charge density between DexS H and DexS L resulted in distinct adsorption capacity and influence the type of adsorption as well as the film surface morphology. For (PAH/DexS H) systems, the high amount of charges on surface due to charges overcompensation leads to the construction of (PAH/DexS H) PEMs with typical symmetric linear growth and homogenous thin films. In contrast, (PAH/DexS L) PEMs present an asymmetric growth between polycation and polyanion adsorption, which suggests a restructuration and a loss of water during LbL process, as it was observed with previous PE couples including synthesized dextrans by Kittle *et al*.[41] As DexS L presents a number of charges per monomer comparable to the number of charges presents on PAH monomer, the restructuration must be due to the partial neutralisation of films and internal diffusion of PEs with adsorption, which contribute to the PEs complexation and dehydration of the system. The effect of restructuration on film surface morphology also influences the film morphology as the formation of PEMs with different pattern is obtained. (PAH/DexS L) PEMs surfaces display "puddle-like" aggregates with pores similar to ones obtained with PE–complex films and microporous membranes based on polysaccharides.[73–75] This work highlights the impact of charge density on the PEMs building and properties at each adsorption step as well as on final aspect of the surface. The possibility to design the surface pattern reminds nano-printing and nano-lithography processes used to fabricate patterns of nanometre scales.[78] In this context, patterning by modulation of PE charge density and LbL process is believed to be a simple method for micro- and nano-patterning especially with the possibility to play with both charge density to build mix-structures with controlled internal and surface morphology based on dextrans sulfates. As it is excepted to obtain different porosity as well as

different colours with the various nanostructures, those systems could help in the development of

colour-based sensors and permeability-controlled nano-objets.

AUTHOR INFORMATION

**Credit authorship contribution statement**

**Aurore Delvart:** Conceptualization, Methodology, Investigation, Analysing Data, Writing-Original Draft & Editing. **Céline Moreau:** Conceptualization, Methodology, Analysing Data, Validation, Writing-Review & editing. **Angélina D'Orlando:** Methodology, Analysing Data, Validation, Writing-review & editing. **Xavier Falourd:** Investigation, Analysing Data, Validation, Writing-review & editing. **Bernard Cathala:** Conceptualization, Methodology, Analysing Data, Writing-review & editing.

All authors have given approval to the final version of the manuscript.

**Declaration of Competing Interest**

The authors declare no competing financial interest or personal relationships that could have appeared to influence the work reported in this paper.

REFERENCES

[1]    E. Díaz-Montes, Dextran: Sources, Structures, and Properties, Polysaccharides. 2 (2021) 554–565. https://doi.org/10.3390/polysaccharides2030033.

[2]    T. Heinze, T. Liebert, B. Heublein, S. Hornig, Functional Polymers Based on Dextran, in: D. Klemm (Ed.), Polysaccharides II, Springer Berlin Heidelberg, 2006: pp. 199–291. https://doi.org/10.1007/12_100.

[3]    E. Antonini, L. Bellelli, M.R. Bruzzesi, A. Caputo, E. Chiancone, A. Rossi-Fanelli, Studies on dextran and dextran derivatives. I. Properties of native dextran in different solvents, Biopolymers. 2 (1964) 27–34. https://doi.org/10.1002/bip.1964.360020105.

[4]    M. Naessens, A. Cerdobbel, W. Soetaert, E.J. Vandamme, Leuconostoc dextransucrase and dextran: production, properties and applications, Journal of Chemical Technology & Biotechnology. 80 (2005) 845–860. https://doi.org/10.1002/jctb.1322.

[5]    T.D. Leathers, Dextran, Biopolymers. 5 (2002) 299–321.

[6]    J.F. Robyt, Dextran. Encyclopaedia of Polymer Science, Wiley-Vch. 4 (1985) 753–767.

[7]    D. de Belder, Polysaccharides in Medicinal Applications, Marcel Dekker, New York. (1996) 505–524.

[8]    W.C. Shoemaker, Comparison of the relative effectiveness of whole blood transfusions and various types of fluid therapy in resuscitation, Critical Care Medicine. 4 (1976). https://journals.lww.com/ccmjournal/Fulltext/1976/03000/Comparison_of_the_relative_eff ectiveness_of_whole.6.aspx.

[9]    W. Richter, Normalizing effect of low molecular weight dextran fractions on the reduced suspension stability of human erythrocytes in vitro, Acta Chir Scand. 131 (1966) 1–8.

[10]   M. Kaisi, E.W.K. Ngwalle, D.E. Runyoro, J. Rogers, Evaluation of tolerance of and response to iron dextran (Imferon [®] ) administered by total dose infusion to pregnant women with iron deficiency anemia, International Journal of Gynecology & Obstetrics. 26 (1988) 235–243. https://doi.org/10.1016/0020-7292(88)90268-8.

[11]   M. Baba, R. Snoeck, R. Pauwels, E. de Clercq, Sulfated polysaccharides are potent and selective inhibitors of various enveloped viruses, including herpes simplex virus, cytomegalovirus, vesicular stomatitis virus, and human immunodeficiency virus, Antimicrob Agents Chemother. 32 (1988) 1742–1745. https://doi.org/10.1128/AAC.32.11.1742.

[12] H. Mitsuya, D. Looney, S. Kuno, R. Ueno, F. Wong-Staal, S. Broder, Dextran sulfate suppression of viruses in the HIV family: inhibition of virion binding to CD4+ cells, Science. 240 (1988) 646–649. https://doi.org/10.1126/science.2452480.

[13] E. Dickinson, M.G. Semenova, Emulsifying properties of covalent protein—dextran hybrids, Colloids and Surfaces. 64 (1992) 299–310. https://doi.org/10.1016/0166-6622(92)80109-F.

[14] R.D. McCurdy, H.D. Goff, D.W. Stanley, A.P. Stone, Rheological properties of dextran related to food applications, Food Hydrocolloids. 8 (1994) 609–623. https://doi.org/10.1016/S0268-005X(09)80068-4.

[15] B. Gelotte, Studies on gel filtration, Journal of Chromatography A. 3 (1960) 330–342. https://doi.org/10.1016/S0021-9673(01)97007-4.

[16] E. Jellum, J. Aaseth, L. Eldjarn, Mercaptodextran, a metal-chelating and disulphide-reducing polythiol of high molecular weight, Biochemical Pharmacology. 22 (1973) 1179–1188. https://doi.org/10.1016/0006-2952(73)90235-9.

[17] T. Serizawa, M. Yamaguchi, M. Akashi, Enzymatic hydrolysis of a layer-by-layer assembly prepared from chitosan and dextran sulfate, Macromolecules. 35 (2002) 8656–8658. https://doi.org/10.1021/ma012153s.

[18] N. Balabushevich, O. Tiourina, D. Volodkin, N. Larionova, G. Sukhorukov, Loading the multilayer dextran sulfate/protamine microsized capsules with peroxidase, Biomacromolecules. 4 (2003) 1191–1197. https://doi.org/10.1021/bm0340321.

[19] L. Pescosolido, W. Schuurman, J. Malda, P. Matricardi, F. Alhaique, T. Coviello, P.R. van Weeren, W.J.A. Dhert, W.E. Hennink, T. Vermonden, Hyaluronic Acid and Dextran-Based Semi-IPN Hydrogels as Biomaterials for Bioprinting, Biomacromolecules. 12 (2011) 1831–1838. https://doi.org/10.1021/bm200178w.

[20] M. Matsusaki, H. Sakaguchi, T. Serizawa, M. Akashi, Controlled release of vascular endothelial growth factor from alginate hydrogels nano-coated with polyelectrolyte multilayer films, Journal of Biomaterials Science-Polymer Edition. 18 (2007) 775–783. https://doi.org/10.1163/156856207781034160.

[21] H. Sakaguchi, T. Serizawa, M. Akashi, Layer-by-layer assembly on hydrogel surfaces and control of human whole blood coagulation, Chemistry Letters. 32 (2003) 174–175. https://doi.org/10.1246/cl.2003.174.

[22] G. Xu, P. Liu, D. Pranantyo, K.-G. Neoh, E.-T. Kang, Dextran- and Chitosan-Based Antifouling, Antimicrobial Adhesion, and Self-Polishing Multilayer Coatings from pH-

Responsive Linkages-Enabled Layer-by-Layer Assembly, ACS Sustainable Chem. Eng. 6 (2018) 3916–3926. https://doi.org/10.1021/acssuschemeng.7b04286.

[23] R. Hashide, K. Yoshida, Y. Hasebe, S. Takahashi, K. Sato, J. Anzai, Insulin-containing layer-by-layer films deposited on poly(lactic acid) microbeads for pH-controlled release of insulin, Colloids and Surfaces B-Biointerfaces. 89 (2012) 242–247. https://doi.org/10.1016/j.colsurfb.2011.09.023.

[24] G. Decher, J.D. Hong, J. Schmitt, Buildup of ultrathin multilayer films by a self-assembly process: III. Consecutively alternating adsorption of anionic and cationic polyelectrolytes on charged surfaces, Thin Solid Films. 210–211 (1992) 831–835. https://doi.org/10.1016/0040-6090(92)90417-A.

[25] G. Decher, Fuzzy Nanoassemblies: Toward Layered Polymeric Multicomposites, Science. 277 (1997) 1232–1237. https://doi.org/10.1126/science.277.5330.1232.

[26] B. Schoeler, G. Kumaraswamy, F. Caruso, Investigation of the Influence of Polyelectrolyte Charge Density on the Growth of Multilayer Thin Films Prepared by the Layer-by-Layer Technique, Macromolecules. 35 (2002) 889–897. https://doi.org/10.1021/ma011349p.

[27] U. Voigt, W. Jaeger, G.H. Findenegg, R. v. Klitzing, Charge Effects on the Formation of Multilayers Containing Strong Polyelectrolytes, J. Phys. Chem. B. 107 (2003) 5273–5280. https://doi.org/10.1021/jp0256488.

[28] J.B. Schlenoff, H. Ly, M. Li, Charge and Mass Balance in Polyelectrolyte Multilayers, J. Am. Chem. Soc. 120 (1998) 7626–7634. https://doi.org/10.1021/ja980350+.

[29] J.B. Schlenoff, S.T. Dubas, Mechanism of Polyelectrolyte Multilayer Growth: Charge Overcompensation and Distribution, Macromolecules. 34 (2001) 592–598. https://doi.org/10.1021/ma0003093.

[30] T. Crouzier, C. Picart, Ion Pairing and Hydration in Polyelectrolyte Multilayer Films Containing Polysaccharides, Biomacromolecules. 10 (2009) 433–442. https://doi.org/10.1021/bm8012378.

[31] N.A. Kotov, Layer-by-layer self-assembly: The contribution of hydrophobic interactions, Nanostructured Materials. 12 (1999) 789–796. https://doi.org/10.1016/S0965-9773(99)00237-8.

[32] C. Cerclier, F. Cousin, H. Bizot, C. Moreau, B. Cathala, Elaboration of Spin-Coated Cellulose-Xyloglucan Multilayered Thin Films, Langmuir. 26 (2010) 17248–17255. https://doi.org/10.1021/la102614b.

[33] C. Picart, J. Mutterer, L. Richert, Y. Luo, G.D. Prestwich, P. Schaaf, J.-C. Voegel, P. Lavalle, Molecular basis for the explanation of the exponential growth of polyelectrolyte multilayers, Proceedings of the National Academy of Sciences. 99 (2002) 12531–12535. https://doi.org/10.1073/pnas.202486099.

[34] C. Picart, Ph. Lavalle, P. Hubert, F.J.G. Cuisinier, G. Decher, P. Schaaf, J.-C. Voegel, Buildup Mechanism for Poly(L-lysine)/Hyaluronic Acid Films onto a Solid Surface, Langmuir. 17 (2001) 7414–7424. https://doi.org/10.1021/la010848g.

[35] F. Boulmedais, V. Ball, P. Schwinte, B. Frisch, P. Schaaf, J.-C. Voegel, Buildup of Exponentially Growing Multilayer Polypeptide Films with Internal Secondary Structure, Langmuir. 19 (2003) 440–445. https://doi.org/10.1021/la0264522.

[36] M. Elzbieciak, M. Kolasińska, S. Zapotoczny, R. Krastev, M. Nowakowska, P. Warszyński, Nonlinear growth of multilayer films formed from weak polyelectrolytes, Colloids and Surfaces A: Physicochemical and Engineering Aspects. 343 (2009) 89–95. https://doi.org/10.1016/j.colsurfa.2009.01.034.

[37] S.T. Dubas, J.B. Schlenoff, Factors Controlling the Growth of Polyelectrolyte Multilayers, Macromolecules. 32 (1999) 8153–8160. https://doi.org/10.1021/ma981927a.

[38] R. v. Klitzing, B. Tieke, Polyelectrolyte Membranes, in: M. Schmidt (Ed.), Polyelectrolytes with Defined Molecular Architecture I, Springer Berlin Heidelberg, Berlin, Heidelberg, 2004: pp. 177–210. https://doi.org/10.1007/b11270.

[39] M. Salomäki, P. Tervasmäki, S. Areva, J. Kankare, The Hofmeister Anion Effect and the Growth of Polyelectrolyte Multilayers, Langmuir. 20 (2004) 3679–3683. https://doi.org/10.1021/la036328y.

[40] J. Schmitt, T. Gruenewald, G. Decher, P.S. Pershan, K. Kjaer, M. Loesche, Internal structure of layer-by-layer adsorbed polyelectrolyte films: a neutron and x-ray reflectivity study, Macromolecules. 26 (1993) 7058–7063. https://doi.org/10.1021/ma00077a052.

[41] J.D. Kittle, H. Wondraczek, C. Wang, F. Jiang, M. Roman, T. Heinze, A.R. Esker, Enhanced Dewatering of Polyelectrolyte Nanocomposites by Hydrophobic Polyelectrolytes, Langmuir. 28 (2012) 11086–11094. https://doi.org/10.1021/la3016996.

[42] F. Höök, B. Kasemo, T. Nylander, C. Fant, K. Sott, H. Elwing, Variations in Coupled Water, Viscoelastic Properties, and Film Thickness of a Mefp-1 Protein Film during Adsorption and Cross-Linking: A Quartz Crystal Microbalance with Dissipation Monitoring, Ellipsometry, and Surface Plasmon Resonance Study, Anal. Chem. 73 (2001) 5796–5804. https://doi.org/10.1021/ac0106501.

[43] M. Salomäki, J. Kankare, Specific Anion Effect in Swelling of Polyelectrolyte Multilayers, Macromolecules. 41 (2008) 4423–4428. https://doi.org/10.1021/ma800315j.

[44] S.T. Dubas, J.B. Schlenoff, Swelling and Smoothing of Polyelectrolyte Multilayers by Salt, Langmuir. 17 (2001) 7725–7727. https://doi.org/10.1021/la0112099.

[45] S.S. Shiratori, M.F. Rubner, pH-Dependent Thickness Behavior of Sequentially Adsorbed Layers of Weak Polyelectrolytes, Macromolecules. 33 (2000) 4213–4219. https://doi.org/10.1021/ma991645q.

[46] A. Davantès, M. Nigen, C. Sanchez, A. d'Orlando, D. Renard, Adsorption of Hyperbranched Arabinogalactan-Proteins from Plant Exudate at the Solid–Liquid Interface, Colloids and Interfaces. 3 (2019) 49. https://doi.org/10.3390/colloids3020049.

[47] J.R. Stokes, L. Macakova, A. Chojnicka-Paszun, C.G. de Kruif, H.H.J. de Jongh, Lubrication, Adsorption, and Rheology of Aqueous Polysaccharide Solutions, Langmuir. 27 (2011) 3474–3484. https://doi.org/10.1021/la104040d.

[48] I.G. Sedeva, D. Fornasiero, J. Ralston, D.A. Beattie, Reduction of Surface Hydrophobicity Using a Stimulus-Responsive Polysaccharide, Langmuir. 26 (2010) 15865–15874. https://doi.org/10.1021/la101695w.

[49] A. Güner, Unperturbed dimensions and the theta temperature of dextran in aqueous solutions, Journal of Applied Polymer Science. 72 (1999) 871–876. https://doi.org/10.1002/(SICI)1097-4628(19990516)72:7<871::AID-APP2>3.0.CO;2-R.

[50] G.A. Neville, P. Rochon, R.N. Rej, A.S. Perlin, Characterization and differentiation of some complex dextran sulfate preparations of medicinal interest, J Pharm Sci. 80 (1991) 239–244. https://doi.org/10.1002/jps.2600800310.

[51] G. Sauerbrey, Verwendung von Schwingquarzen zur Wägung dünner Schichten und zur Mikrowägung, Z. Physik. 155 (1959) 206–222. https://doi.org/10.1007/BF01337937.

[52] F. Höök, M. Rodahl, P. Brzezinski, B. Kasemo, Energy Dissipation Kinetics for Protein and Antibody−Antigen Adsorption under Shear Oscillation on a Quartz Crystal Microbalance, Langmuir. 14 (1998) 729–734. https://doi.org/10.1021/la970815u.

[53] T. Serizawa, M. Yamaguchi, T. Matsuyama, M. Akashi, Alternating Bioactivity of Polymeric Layer-by-Layer Assemblies: Anti- vs Procoagulation of Human Blood on Chitosan and Dextran Sulfate Layers, Biomacromolecules. 1 (2000) 306–309. https://doi.org/10.1021/bm000006g.

[54] E. Stenberg, B. Persson, H. Roos, C. Urbaniczky, Quantitative determination of surface concentration of protein with surface plasmon resonance using radiolabeled proteins, Journal

of Colloid and Interface Science. 143 (1991) 513–526. https://doi.org/10.1016/0021-9797(91)90284-F.

[55] J.A.D. Feijter, J. Benjamins, F.A. Veer, Ellipsometry as a tool to study the adsorption behavior of synthetic and biopolymers at the air–water interface, Biopolymers. 17 (1978) 1759–1772. https://doi.org/10.1002/bip.1978.360170711.

[56] J. Kittle, J. Levin, N. Levin, Water Content of Polyelectrolyte Multilayer Films Measured by Quartz Crystal Microbalance and Deuterium Oxide Exchange, Sensors. 21 (2021) 771. https://doi.org/10.3390/s21030771.

[57] A. Villares, H. Bizot, C. Moreau, A. Rolland-Sabaté, B. Cathala, Effect of xyloglucan molar mass on its assembly onto the cellulose surface and its enzymatic susceptibility, Carbohydrate Polymers. 157 (2017) 1105–1112. https://doi.org/10.1016/j.carbpol.2016.10.072.

[58] S. Anandhakumar, A.M. Raichur, A facile route to synthesize silver nanoparticles in polyelectrolyte capsules, Colloids and Surfaces B-Biointerfaces. 84 (2011) 379–383. https://doi.org/10.1016/j.colsurfb.2011.01.029.

[59] J. Sripriya, S. Anandhakumar, S. Achiraman, J.J. Antony, D. Siva, A.M. Raichur, Laser receptive polyelectrolyte thin films doped with biosynthesized silver nanoparticles for antibacterial coatings and drug delivery applications, International Journal of Pharmaceutics. 457 (2013) 206–213. https://doi.org/10.1016/j.ijpharm.2013.09.036.

[60] J.M.C. Lourenço, P.A. Ribeiro, A.M. Botelho do Rego, F.M. Braz Fernandes, A.M.C. Moutinho, M. Raposo, Counterions in Poly(allylamine hydrochloride) and Poly(styrene sulfonate) Layer-by-Layer Films, Langmuir. 20 (2004) 8103–8109. https://doi.org/10.1021/la049872v.

[61] C. Moreau, N. Beury, N. Delorme, B. Cathala, Tuning the Architecture of Cellulose Nanocrystal–Poly(allylamine hydrochloride) Multilayered Thin Films: Influence of Dipping Parameters, Langmuir. 28 (2012) 10425–10436. https://doi.org/10.1021/la301293r.

[62] C. Elosua, D. Lopez-Torres, M. Hernaez, I.R. Matias, F.J. Arregui, Comparative study of layer-by-layer deposition techniques for poly(sodium phosphate) and poly(allylamine hydrochloride), Nanoscale Research Letters. 8 (2013) 539. https://doi.org/10.1186/1556-276X-8-539.

[63] M. Elżbieciak-Wodka, M. Kolasińska-Sojka, P. Nowak, P. Warszyński, Comparison of permeability of poly(allylamine hydrochloride)/and poly(diallyldimethylammonium chloride)/poly(4-styrenesulfonate) multilayer films: Linear vs. exponential growth, Journal

of Electroanalytical Chemistry. 738 (2015) 195–202. https://doi.org/10.1016/j.jelechem.2014.11.035.

[64] F. Caruso, K. Niikura, D.N. Furlong, Y. Okahata, 1. Ultrathin Multilayer Polyelectrolyte Films on Gold: Construction and Thickness Determination, Langmuir. 13 (1997) 3422–3426. https://doi.org/10.1021/la960821a.

[65] E.M. Pinto, M.M. Barsan, C.M.A. Brett, Mechanism of Formation and Construction of Self-Assembled Myoglobin/Hyaluronic Acid Multilayer Films: An Electrochemical QCM, Impedance, and AFM Study, J. Phys. Chem. B. 114 (2010) 15354–15361. https://doi.org/10.1021/jp107107b.

[66] M.M. de Villiers, D.P. Otto, S.J. Strydom, Y.M. Lvov, Introduction to nanocoatings produced by layer-by-layer (LbL) self-assembly, Advanced Drug Delivery Reviews. 63 (2011) 701–715. https://doi.org/10.1016/j.addr.2011.05.011.

[67] E.J. Calvo, V. Flexer, M. Tagliazucchi, P. Scodeller, Effects of the nature and charge of the topmost layer in layer by layer self assembled amperometric enzyme electrodes, Phys. Chem. Chem. Phys. 12 (2010) 10033–10039. https://doi.org/10.1039/C0CP00449A.

[68] R.A. Ghostine, M.Z. Markarian, J.B. Schlenoff, Asymmetric Growth in Polyelectrolyte Multilayers, J. Am. Chem. Soc. 135 (2013) 7636–7646. https://doi.org/10.1021/ja401318m.

[69] Z. Jaafar, K. Mazeau, A. Boissière, S. Le Gall, A. Villares, J. Vigouroux, N. Beury, C. Moreau, M. Lahaye, B. Cathala, Meaning of xylan acetylation on xylan-cellulose interactions: A quartz crystal microbalance with dissipation (QCM-D) and molecular dynamic study, Carbohydrate Polymers. 226 (2019) 115315. https://doi.org/10.1016/j.carbpol.2019.115315.

[70] E.G. Towle, I. Ding, A.M. Peterson, Impact of molecular weight on polyelectrolyte multilayer assembly and surface properties, Journal of Colloid and Interface Science. 570 (2020) 135–142. https://doi.org/10.1016/j.jcis.2020.02.114.

[71] N. Ghavidel Mehr, C.D. Hoemann, B.D. Favis, Chitosan surface modification of fully interconnected 3D porous poly(ε-caprolactone) by the LbL approach, Polymer. 64 (2015) 112–121. https://doi.org/10.1016/j.polymer.2015.03.025.

[72] N. Barroso, O. Guaresti, L. Pérez-Álvarez, L. Ruiz-Rubio, N. Gabilondo, J.L. Vilas-Vilela, Self-healable hyaluronic acid/chitosan polyelectrolyte complex hydrogels and multilayers, European Polymer Journal. 120 (2019) 109268. https://doi.org/10.1016/j.eurpolymj.2019.109268.

[73] W. Liu, S. Wijeratne, L. Yang, M. Bruening, Porous star-star polyelectrolyte multilayers for protein binding, Polymer. 138 (2018) 267–274. https://doi.org/10.1016/j.polymer.2018.01.055.

[74] A. Hollman, D. Bhattacharyya, Pore assembled multilayers of charged polypeptides in microporous membranes for ion separation, Langmuir. 20 (2004) 5418–5424. https://doi.org/10.1021/la049688+.

[75] Y. Fu, S. Bai, S. Cui, D. Qiu, Z. Wang, X. Zhang, Hydrogen-Bonding-Directed Layer-by-Layer Multilayer Assembly: Reconformation Yielding Microporous Films, Macromolecules. 35 (2002) 9451–9458. https://doi.org/10.1021/ma0207881.

[76] Q. Feng, G. Zeng, P. Yang, C. Wang, J. Cai, Self-assembly and characterization of polyelectrolyte complex films of hyaluronic acid/chitosan, Colloids and Surfaces A: Physicochemical and Engineering Aspects. 257–258 (2005) 85–88. https://doi.org/10.1016/j.colsurfa.2004.10.099.

[77] K. Glinel, A. Moussa, A.M. Jonas, A. Laschewsky, Influence of Polyelectrolyte Charge Density on the Formation of Multilayers of Strong Polyelectrolytes at Low Ionic Strength, Langmuir. 18 (2002) 1408–1412. https://doi.org/10.1021/la0113670.

[78] N. Vigneswaran, F. Samsuri, B. Ranganathan, Padmapriya, Recent Advances in Nano Patterning and Nano Imprint Lithography for Biological Applications, Procedia Engineering. 97 (2014) 1387–1398. https://doi.org/10.1016/j.proeng.2014.12.420.

**1. PAH**

**2. Rising**

**3. DexS**

**4. Rising**

1 layer

1 bilayer

× 10

10 bilayers

**DexS H**
high charge density

DexS 10

**DexS L**
low charge density

DexS 10